CT-based geometry analysis and finite element models of the human and ovine bronchial tree

Merryn H. Tawhai, Peter Hunter, Juerg Tschirren, Joseph Reinhardt, Geoffrey McLennan and Eric A. Hoffman

J Appl Physiol 97:2310-2321, 2004. First published 20 August 2004;
doi: 10.1152/japplphysiol.00520.2004

J Appl Physiol 97: 2310–2321, 2004.
First published August 20, 2004; doi:10.1152/japplphysiol.00520.2004.

CT-based geometry analysis and finite element models of the human and ovine bronchial tree

Merryn H. Tawhai,[1] Peter Hunter,[1] Juerg Tschirren,[2] Joseph Reinhardt,[3] Geoffrey McLennan,[3,4] and Eric A. Hoffman[2,3]

[1]*Bioengineering Institute, The University of Auckland, 92019 Auckland, New Zealand; Departments of* [2]*Radiology and* [3]*Biomedical Engineering, and* [4]*Medicine, University of Iowa, Iowa City, Iowa 52242*

Submitted 27 May 2004; accepted in final form 17 August 2004

Tawhai, Merryn H., Peter Hunter, Juerg Tschirren, Joseph Reinhardt, Geoffrey McLennan, and Eric A. Hoffman. CT-based geometry analysis and finite element models of the human and ovine bronchial tree. *J Appl Physiol* 97: 2310–2321, 2004. First published August 20, 2004; doi:10.1152/japplphysiol.00520.2004.—The interpretation of experimental results from functional medical imaging is complicated by intersubject and interspecies differences in airway geometry. The application of computational models in understanding the significance of these differences requires methods for generation of subject-specific geometric models of the bronchial airway tree. In the current study, curvilinear airway centerline and diameter models have been fitted to human and ovine bronchial trees using detailed data segmented from multidetector row X-ray-computed tomography scans. The trees have been extended to model the entire conducting airway system by using a volume-filling algorithm to generate airway centerline locations within detailed volume descriptions of the lungs or lobes. Analysis of the geometry of the scan-based and model-based airways has verified their consistency with measures from previous anatomic studies and has provided new anatomic data for the ovine bronchial tree. With the use of an identical parameter set, the volume-filling algorithm has produced airway trees with branching asymmetry appropriate for the human and ovine lung, demonstrating the dependence of the method on the shape of the lung or lobe volume. The modeling approach that has been developed can be applied to any level of detail of the airway tree and into any volume shape for the lung; hence it can be used directly for different individuals or animals and for any number of scan-based airways. The resulting models are subject-specific computational meshes with anatomically consistent geometry, suitable for application in simulation studies.

computed tomography

MATHEMATICAL MODELS of the bronchial tree have been used extensively for computational simulations of pulmonary function. The classic airway models of Weibel (43) and Horsfield et al. (10) are appropriate for investigations where the effect of airway branching asymmetry can be neglected or where asymmetry does play a significant role but the spatial location of airways can be neglected (28). When both the branching asymmetry and the spatial position of the airways are important (40), a different class of bronchial airway model is required. These anatomically based models, derived from patient medical imaging data, are specific to any number of imaged individuals rather than seeking to be representative of a population. For example, Tawhai et al. (37) modeled the human bronchial airway system by filling a finite element volume mesh of the five human lobes with a bifurcating-distributive tree. The algorithm generated a tree into the individual lobes, starting from each predefined lobar bronchus. The method was shown to produce a bronchial tree with branching pattern and geometry representative of measurements from casts of the lung (37). The bronchial tree model has been applied in simulations of inert gas mixing (38) and airway thermodynamics (39). Although others have similarly attempted to generate bronchial tree models (16), we are not aware of similar methods having been applied to generate anatomically based, spatially distributed models of the bronchial tree in other species.

The human bronchial tree has an asymmetric branching pattern, but it is more symmetric than other mammalian lungs (32). The human airways tend to form distinct bifurcations into two child airways with generally different diameters, lengths, and branching angles (32). In contrast, the ovine (sheep) bronchial tree has a monopodial branching pattern that is typical of most mammalian species other than *Homo sapiens*. In monopodial branching, the parent airway tends to give rise to a minor child branch at a large branching angle and a major child branch at a much smaller angle (13). An example of this branching pattern is the bronchus that arises directly from the sheep trachea to supply the right apical lobe. By definition the right apical lobe bronchus is the minor child of the upper portion of the trachea, and the continuation of the trachea beyond the branch point is the major child. The monopodial branching pattern produces a more asymmetric bronchial tree with respect to the rate of increase of the number of branches and the rates of decrease of branch length and diameter with each branch division.

The differences between the human and sheep airways in branching pattern and dimension may influence the interpretation of experimental results from sheep in terms of their implication for the human lung. For example, predictions of the location of deposition of particles or the rate of transfer of heat and moisture (39) will both be influenced by the species-specific geometry. Recent studies in which computed tomography (CT) and MRI methods are being used to study regional ventilation (1, 19, 20, 21, 35, 36) and perfusion (2, 3, 44, 45) make use of gases of considerably different densities and viscosities (xenon and helium), both of which differ significantly from that of room air. As we seek to build a normative atlas of the human and animal lungs for the purpose of detecting and quantitatively following disease (7, 8), there is a growing interest in subject-specific models of the pulmonary airway and vascular trees. These models will aid in the ability

Address for reprint requests and other correspondence: M. Tawhai, Bioengineering Institute, The Univ. of Auckland, Private Bag 92019, Auckland, New Zealand (E-mail: m.tawhai@auckland.ac.nz).

The costs of publication of this article were defrayed in part by the payment of page charges. The article must therefore be hereby marked "*advertisement*" in accordance with 18 U.S.C. Section 1734 solely to indicate this fact.

to interrogate model-based hypotheses regarding the principles that govern the regional distribution of ventilation and perfusion, with the ability to evaluate the model predictions by comparison with in vivo measures based on imaging of the individual from whom the model was constructed. Anatomic customized models of different individuals or different species can be used to probe the sensitivity of predictions to differences in geometry, whether subtle (normal temporal change in airway caliber of an individual) or major (between species).

In the current study, models of the human and sheep bronchial trees are derived directly from detailed anatomic data obtained from multidetector row X-ray-CT (MDCT) scans. The models represent the curvilinear centerlines and cross-sectional areas of individual airways in an efficient format. The human MDCT airway models extend from the trachea to a maximum of *generation 10*, and the sheep MDCT airway models extend from the trachea to a maximum of *generation 23* (because of the monopodial nature of the sheep airway, generation number can grow rapidly along the major dorsal-basal conducting path). Volume meshes of the sheep lungs and human lobes are fitted to MDCT data from the lung or lobe surface, and the method of Tawhai et al. (37) is extended and applied for generating anatomically based airway models that start from the periphery of the MDCT-segmented airways and fill the volume meshes. The geometry of the MDCT-based and algorithm-based models are each analyzed to *1*) verify the accuracy of the MDCT segmentation algorithms in identifying airway location and geometry and *2*) verify the appropriateness of the airway generation algorithm for generating bronchial trees for the human and sheep lung. The current study also provides new data on the geometry of the human and sheep bronchial airway trees.

Ordering Schemes

The bronchial trees are classified by generations and by two ordering schemes. Generations count downward from a stem branch, with each child branch one generation higher than its parent. In the current study the trachea is classified as *generation 1*.

Horsfield ordering classifies the peripheral conducting airways [transitional bronchioles as defined by Haefeli-Bleuer and Weibel (5)] as *order 1*, and, moving back toward the stem branch, each parent is one order higher than the child branch of highest order. Strahler ordering also classifies the terminal branches as *order 1*. The order of a parent branch is one higher than two child branches of the same order or else the same as the child branch of highest order. In Strahler ordering, any series of branches that are of the same order are considered to be a single branch.

Any portion of a treelike structure can be classified by generations, but classification by orders requires knowledge of the entire tree, or a scheme designed to assign orders based on, for example, the diameter range (26). Weibel generations and Horsfield and Strahler ordering are all used to classify trees in the current analysis so that comparisons can be made with corresponding generation- or order-based measures from anatomic studies. Because Strahler ordering is more appropriate for branch divisions where the distinction between parent and child branch may not be clear, this is the ordering system that is used preferentially in the current study.

Indexes of Asymmetry

The rate of decrease in length or diameter with decreasing order, or rate of increase in the number of branches, can be characterized by the length, diameter, and branching ratios, respectively (11). The branching ratio (R_b) is the antilog of the slope of log(number of branches) plotted against order. The length ratio (R_l) and diameter ratio (R_d) are calculated similarly from the plots of log(mean length) or log(mean diameter) against order. R_b, R_l, and R_d can be calculated using either Horsfield or Strahler ordering. In the current study, the Horsfield-based ratios are suffixed by H (R_bH, R_lH, R_dH) and the Strahler-based ratios are suffixed by S (R_bS, R_lS, R_dS). A tree with $R_bS = R_bH = 2$ has a symmetric branching pattern; asymmetric trees have lower R_bH and higher R_bS.

METHODS

Imaging Protocol

Human studies were approved by the University of Iowa Institutional Review Board and Radiation Safety Committees. Animal studies were approved by the University of Iowa Animal Care and Use Committee.

Imaging of the subjects presented in this paper was performed in the supine body posture for the human subject and prone for the sheep, with lungs held at 90% vital capacity (human) or total lung capacity (TLC; sheep). Sheep were kept anesthetized via pentobarbital sodium, and the human subject was unsedated. Lung volume was controlled via use of a custom-built pneumotachometer-based lung volume control device. The device closed a balloon valve at the mouth under computer control when the subject reached the desired lung volume on expiration after a full inspiration to TLC (25 cmH_2O airway pressure). Spiral scanning was performed using an MDCT Scanner (Marconi MX8000) with a pitch of 1.5, collimation of 1.2, 100 mAs, 120 kV, slice thickness of 1.3 mm, slice increment of 0.65 mm, a reconstruction matrix size of 512 × 512, and a field of view of ~35 cm for humans and 28 cm for sheep.

Segmentation Skeletonization and Anatomic Measurements

Lungs, lobes (humans only), and airway trees were automatically segmented (extracted) using custom-built software. Hu et al. (14) and Shi et al. (34) detail the segmentation process used for the human and sheep lungs respectively, and Zhang et al. (44) describe that used for the human lobes. The current study is concerned primarily with identification of the airway tree.

An airway segmentation algorithm (41, 42) based on multiseeded fuzzy connectivity (6) was used to identify the airway locations. Segmentation was performed in small cylindrical regions of interest (ROI). These ROIs adaptively followed the airway segments as they were segmented. This approach has three advantages.

First, the segmentation is kept within a small and therefore controllable area. With this approach it is possible to automatically detect problems such as leaks into the surrounding lung parenchyma (erroneous labeling of lung parenchyma as airway lumen) at their root. Appropriate countermeasures can be taken without the need for any user interaction (41, 42).

Second, the algorithm can automatically adapt to changing image properties such as gradients and varying noise content.

Third, reduction of the size of the segmentation space and the division of the overall problem size into small subproblems results in a moderate computing time.

Segmentation of the human and sheep airway trees from the subjects in the current study are shown in Fig. 1.

The skeleton of the segmented airway trees was found by applying a sequential thinning algorithm (23). The skeletal line resulting from

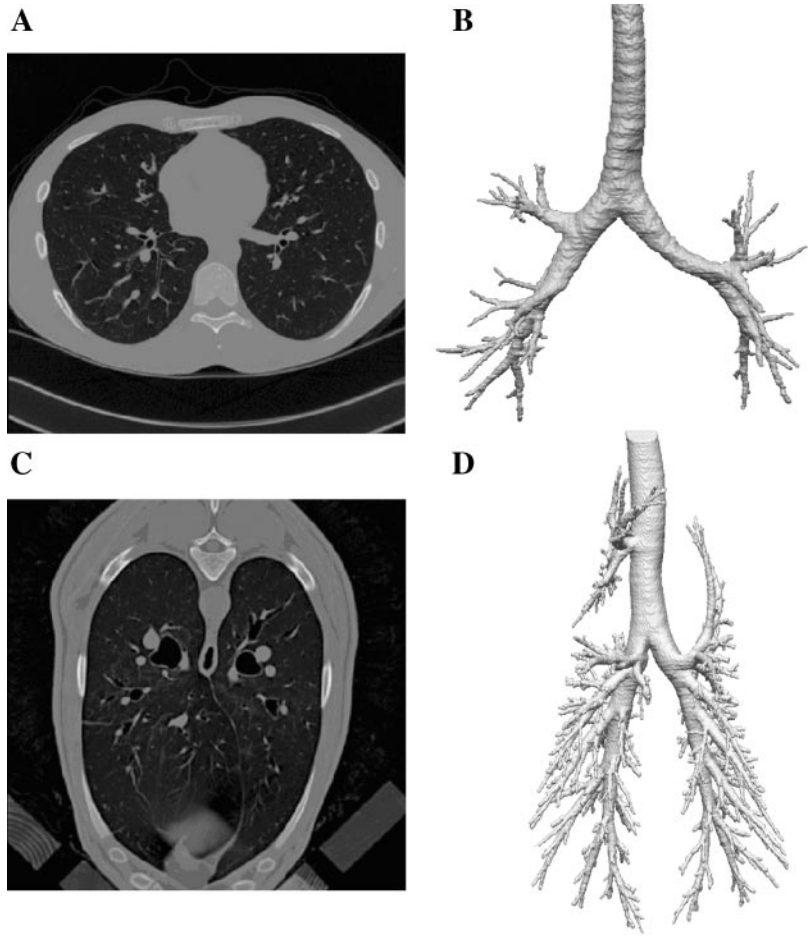

Fig. 1. A single multidetector row X-ray-computed tomography (MDCT) cross-sectional image from the supine human subject (*A*) and 3-dimensional (3D) reconstruction of masked airways from the same human subject (*B*). Single MDCT image from the prone sheep (*C*) and masked 3D airway reconstruction for the same subject (*D*).

this algorithm is guaranteed to lie in the center of the airway segments, and the branchpoints are located at their correct anatomic locations (24).

Anatomic measurements (minor and major diameter, cross-sectional area) were made in the original gray-level MDCT volume (41). Measurements were conducted in two-dimensional slices that were resampled perpendicular to the segment's centerline. Only the cylindrical parts of the respective airway segment were considered: the branchpoint regions were excluded. An independent set of measurements was taken at every centerline voxel position. The method has been demonstrated to achieve subvoxel accuracy (typical error ~0.1 mm) on a Plexiglas phantom, independent of airway orientation and X-ray dose (41).

The measured tree geometry was stored in an XML (eXtensible Markup Language) "tree file." The tree file records the location of each bifurcation point, how the bifurcation points are linked to form the skeleton, the location of multiple discrete centerline points that trace the path of the airway centerline along each airway segment, and the cross-sectional area of the airway orthogonal to each centerline point.

Derivation of Centerline Models for Segmented Airways

Finite element models of the segmented airway trees were derived directly from the information stored in the XML tree file. Each bifurcation point was translated into a finite element "node," and the tree file connectivity was translated into finite element mesh connectivity (a set of connected "elements"). Each element contained only two nodes (hence a 1-dimensional mesh), and the initial geometry was that of a linear mesh (straight lines joining adjacent bifurcation points). The location of the bifurcation points did not change during the fitting process, but the curvature of the elements changed to provide a best fit to the centerline locations. That is, the mesh that was fitted to the centerline points was comprised of "high-order" elements that included derivative information at the nodes.

The locations of centerline points from the tree file were translated to data points for geometry fitting. The centerline points were used to fit curvature to the one-dimensional mesh, such that the distance between the mesh location and the points was minimized. Details of the generalized geometry fitting technique can be found in Fernandez et al. (4). The technique is summarized as follows specifically for the centerline fit.

Step 1. The orthogonal projection of each centerline point to its corresponding element is calculated. These minimum distances are summed to estimate the error in the fit.

Step 2. The sum of the projections, written in terms of nodal coordinates and derivatives, is the objective function that the solution seeks to minimize. For each element in the mesh a linear system of equations is generated by differentiating the objective function with respect to each element parameter and equating the resulting expression to zero.

Step 3. The system of equations is solved for new derivative values to minimize the objective function and excessive element curvature.

Step 4. Steps 1–3 are repeated until the solution converges and the error is small. That is, because the mesh curvature changes during the solution the orthogonal projections are recalculated and an updated objective function formulated for solution.

The initial linear tree was fitted to the centerline point data to produce a curvilinear mesh with deliberate derivative discontinuities at the nodes. That is, the mesh included curvature information for each

airway but the curvature from a parent to a child airway may change abruptly, hence the mesh fitting was not constrained to preserve derivative continuity. This is in contrast to the general application of the geometry fitting technique to biological structures (4), where preservation of derivative continuity is essential to accurately represent surface curvature.

Fitting Area Data to the Centerline Models

The XML tree file provides data for the cross-sectional area and major and minor elliptical diameters orthogonal to the centerline points. The orientation of the elliptical section is not defined, hence a cylindrical cross section was assumed for the current model derivation and geometry analysis.

The circular diameters calculated from the cross-sectional areas were translated to data values, each associated with a unique centerline point location, for fitting to the centerline mesh. The mean diameter for an airway was used to define the initial diameter of the corresponding mesh element. That is, the initial diameter values were constant along an element and discontinuous at the nodes. Each node stored up to three versions of the diameter: one for each connected element. The diameter along the elements was fitted to the initial mesh using a similar technique to that described for fitting the geometry of the mesh, but in this case the objective function was formed from the sum of the differences between the centerline point diameter values and the corresponding interpolated diameters in terms of nodal values and derivatives. The diameter quantities were fitted to the set of diameter data to minimize the objective function. Because the system was linear and no updating of values was required, the solution took only a single iteration.

Generation of Centerline Model by Algorithm

The airway generation algorithm developed by Tawhai et al. (37) was used to generate an airway model starting from the MDCT-based airway geometry and terminating at the terminal bronchioles, for the human and sheep lung. Airways were generated into MDCT-based volume meshes of the lobes (human) or lungs (sheep) derived from data from the same MDCT scans that were used to construct the XML tree files. The volume meshes were constructed by geometry fitting of lung or lobe surface MDCT data to high-order volume elements (4).

A grid of uniformly spaced seed points was calculated to lie within each lobe or lung, with density equal to the estimated density of the transitional bronchioles. The density for both human and sheep was estimated using the expected number of transitional bronchioles in the human lung (~30,000) (5) divided by the lung volume. The human lung volume was 7.05 liters at ~90% vital capacity and the sheep lung volume was 2.88 liters at close to TLC, hence the transitional bronchiole density of the sheep lung was over twice that of the human density.

With the use of the peripheral airways in the MDCT-based airway models as starting elements for mesh generation, the algorithm proceeds as follows.

Step 1. The closest peripheral branch end point is calculated for each seed point; hence there are initially N sets of seed points for the N peripheral airways in the MDCT-based model.

Step 2. The center of mass of each set of points is calculated as the average of the seed point spatial coordinates.

Step 3. Each set of points is divided into two sets of generally unequal size by the plane that contains both the center of mass and the two nodes of the parent branch.

Step 4. The center of mass of each new set of points is calculated.

Step 5. For each set of points an airway is generated to start at the end of the parent branch, directed toward the center of mass. The length of the new branch is 40% of the distance from the end of the parent to the center of mass (37).

Step 6. Each set of points is checked to determine whether the generated branch is terminal; a terminal branch arises when the set contains only a single seed point, or the branch length is less than a minimum length. For any terminal branch the single seed point remaining (or closest seed point to the terminal node for a length-limited branch) is removed from the global set of seed points.

Step 7. Steps 1–6 are repeated until no seed points remain.

Estimates of the length of the human transitional bronchiole range from ~1.5 (5) to 1.72 mm (25). Direct measurements of the length of the transitional bronchiole in the sheep are not currently available. A value of 2 mm was therefore used for the length limit for both the human and sheep models.

For analysis in the current study the diameters in the generated airways were calculated by assuming that $R_dS = R_bS^{1/3}$ (11). The full generated tree was first classified by Strahler order, then R_bS was calculated, and *Eq. 1* was used to compute diameters of constant value along a branch:

$$\log D(x) = (x - N) \log R_dS + \log D_N \quad (1)$$

where D is the computed diameter for any branch of order x, x is the Strahler order, N is the highest order (the order of the trachea), and D_N is the diameter of the branch of highest order.

Geometry Analysis

The following assumptions and definitions were used for analysis of the branching pattern and geometry of the bronchial tree data and models.

First, the branching angle (θ) is the angle between the forward directions of the parent and child branches.

Second, the rotation angle (ϕ) is the angle between the plane that contains the parent branch and its sibling and the plane that contains the child branch and its sibling.

Third, the branch diameter for MDCT-measured airways is its average value between 25 and 75% of the branch length; for generated airways, diameter is equal to the value calculated using *Eq. 1*.

Fourth, a minor branch is defined as the child branch with the smallest diameter; a major branch is defined as the child branch with the largest diameter. For two child branches of equal diameter, the minor branch is defined as the child with the largest branching angle.

Geometry analysis was performed on the human and sheep models generated from the full set of MDCT-based airway centerlines, into the five separate lobes (human) or two lungs (sheep). Branching ratios were also calculated for the following airway models: human airways generated into two lungs (merged lobes) from the full MDCT airways; human airways generated into two lungs initiating from the two major bronchi; sheep airways generated from the two major bronchi and the right apical lobe bronchus; and sheep airways generated using a length limit of 3 mm. These extra model generations were performed to check the influence of host geometry and the extent of initial (MDCT) airway definition on the generated asymmetry of the model.

RESULTS

MDCT Airways: Geometry

Figure 1, *B* and *D*, shows three-dimensional rendered isosurfaces for the airways segmented from the MDCT images of the normal human male and sheep, respectively. One hundred twenty-one individual airways were identified from the human images, whereas segmentation of the sheep images identified 933 airways classified by generation or 567 classified by Strahler order. Peripheral segmented airways are in *generations 4* to *10* for the human tree (mean *generation 7.13*) and *generations 5* to *23* for the sheep tree (mean *generation 12.77*). The mean peripheral airway diameters are 2.98 mm (human) and 2.03 mm (sheep).

Tables 1 and 2 list geometric parameters evaluated for all segmented airways from the MDCT-imaged human and sheep

Table 1. *Analysis of the geometry of human MDCT-segmented airways and volume-filling airway model*

	MDCT	Model	Published
θ (Total)	36.11°±20.85°	50.31°±28.92°	37.28° (9); 39°, 43° (30)
θ (D_{parent} 4 mm)	33.98°	33.71°	32° (10)
θ (4 mm>D_{parent} 3 mm)	41.06°	36.72°	30° (10)
θ (3 mm>D_{parent} 2 mm)		45.19°	36° (10)
θ (2 mm>D_{parent} 1 mm)		53.34°	43° (10)
θ (1 mm>D_{parent} 0.7 mm)			50° (10)
ϕ	76.05°±45.73°	89.99°±43.28°	79° (30); 90° (13)
θ_{minor}	36.60°±19.54°	53.00°±29.02°	
θ_{major}	35.53°±22.32°	47.63°±28.56°	
L/D	3.04±2.20	2.92±0.92	3.09, 3.14 (30); 2.8–3.25 (43)
L/D minor child	3.63±2.57	2.88±0.94	2.96±0.97 (27)*
L/D major child	2.48±1.79	2.96±0.90	2.71±1.13 (27)*
D_{minor}/D_{major}	0.85±0.14	0.81±0.17	0.82, 0.74 (30); 0.86 (25, 43)
D/D_{parent}	0.71±0.14	0.79±0.15	0.83, 0.78 (30); 0.79 (43); 0.76 (17)
$\%D/D_{parent}<1$	96.97	99.99	90.6% (17)
D_{minor}/D_{parent}	0.66±0.12	0.69±0.06	
D_{major}/D_{parent}	0.79±0.12	0.88±0.14	0.86 (27)
L/L_{parent}	1.18±1.20	0.81±0.30	0.94±1.37 (17)
$\%L/L_{parent}<1$	61.98	77.94	71.9% (17)
L_1/L_2 ($L_1<L_2$)	0.52±0.23	0.68±0.20	0.58 (30); 0.62 (25, 43)
R_bS		2.80 (R^2 = 1.00)	2.51–2.81 (12)
R_1S		1.39 (R^2 = 0.95)	1.33–1.46 (12)
R_dS		1.41 (R^2 = 0.98)	1.35–1.45 (12)
R_bH		1.47 (R^2 = 0.99)	1.38 (10)
R_1H		1.13 (R^2 = 0.87)	1.11 ($=1.38^{1/3}$)

Results are means ± SD. Values from anatomic studies in the final column are followed by their reference in parentheses *MDCT, multidector row X-ray-computed tomography; L/D, length-to-diameter ratio; R_b, R_l, R_d, branching, length, and diameter ratios using Strahler (S) or Horsfield (H) ordering; θ, branching angle; ϕ, rotation angle. *For 0.8 mm D < 7.2 mm.

lungs, respectively. The final column in each table lists values from anatomic or theoretical studies for comparison.

Although the mean θ (branch angle) calculated from the human MDCT data is only slightly smaller than previously published values, θ calculated by first grouping the branches according to the size of the parent diameter are larger than values published by Horsfield et al. (10). The mean θ calculated from the sheep MDCT data is close to that calculated for the human, and classification by the size of the parent diameter gives θ values that increase for decreasing parent size. This trend is consistent with measurements for the human lung (10).

Mean values for θ_{minor} (branching angle of minor child) and θ_{major} (branching angle of major child) are ~0.5° greater and less than the total mean θ, respectively, for the human MDCT data. The corresponding difference for the sheep is ~10°; that is, a 1° and 20° range (θ_{major}-θ_{minor}) for the human and sheep

Table 2. *Analysis of the geometry of sheep MDCT-segmented airways and volume-filling airway model*

	CT	Model	Published
θ (Total)	35.88°±22.32°	53.71°±27.47°	
θ (D_{parent} 4 mm)	34.83°	36.73°	
θ (4 mm>D_{parent} 3 mm)	36.18°	47.99°	
θ (3 mm>D_{parent} 2 mm)	52.97°	51.02°	
θ (2 mm>D_{parent} 1 mm)		55.85°	
ϕ	89.04°±44.64°	90.17°±40.26°	
θ_{minor}	45.99°±21.94°	56.36°±27.12°	
θ_{major}	25.17°±16.85°	51.16°±27.58°	
L/D	2.69±1.76	2.68±0.90	
L/D_{minor}	2.92±2.15	2.79±0.84	
L/D_{major}	2.33±1.49	2.56±0.92	
D_{minor}/D_{major}	0.72±0.18	0.74±0.22	
D/D_{parent}	0.71±0.18	0.75±0.19	0.75±0.19 (17)*
$\%D/D_{parent}<1$	90.35	99.99	
D_{minor}/D_{parent}	0.61±0.12	0.62±0.11	
D_{major}/D_{parent}	0.86±0.12	0.88±0.16	0.90 (27)†
L/L_{parent}	1.03±0.74	0.83±0.31	
$\%L/L_{parent}<1$	58.95	76.72	
L_1/L_2 ($L_1<L_2$)	0.65±0.23	0.72±0.19	
R_bS		3.19 (R^2 = 1.00)	3.533, 3.565 (12)
R_1S		1.43 (R^2 = 0.87)	1.508, 1.387 (12)
R_dS		1.47 (R^2 = 1.00)	1.666, 1.712 (12)

Results are means ± SD. CT, computed tomography. Values from anatomic studies in the final column are followed by their reference in parentheses. *Dog, rat, hamster; †dog.

branching angles. This agrees with previous observations that the human airway tree is more symmetric with respect to branching angle (32) and that the monopodial airway tree in animals such as the sheep has a large difference between the major and minor branching angle.

Figure 2, *A* and *B*, plot cumulative D/D_{parent} (values up to and including the current generation) and the ratios of minor child to parent diameter (D_{minor}/D_{parent}) and major child to parent diameter (D_{major}/D_{parent}) against parent generation for human (Fig. 2*A*) and sheep (Fig. 2*B*) MDCT airway bifurcations. The mean of the ratios of D/D_{parent} for the human MDCT airways is smaller than reported from previous studies (17, 31, 43): for *generations 1–4*, the cumulative mean value is within the range of published values, D/D_{parent} decreases steadily through *generations 4–6*, then is close to the total mean value up to *generation 10*. The mean D/D_{parent} for the sheep MDCT airways (0.71 ± 0.18) is smaller than reported by Krause et al. (17) for dog bronchial airways (0.75 ± 0.19) based on an analysis of data from Raabe et al. (29). The curves in Fig. 2*B* for cumulative mean values show little change beyond *generation 5* for D/D_{parent}, D_{major}/D_{parent}, and D_{minor}/D_{parent} for the sheep. In contrast to the human bifurcations, the sheep bronchial tree has a significant number of divisions where the major, and occasionally the minor, child has a larger diameter than the parent ($D/D_{parent} > 1$ in Fig. 2*B*). The mean D/D_{parent} values calculated for human and sheep are the same, but D_{minor}/D_{parent} for the sheep is less than for human, and D_{major}/D_{parent} is greater for the sheep than for human.

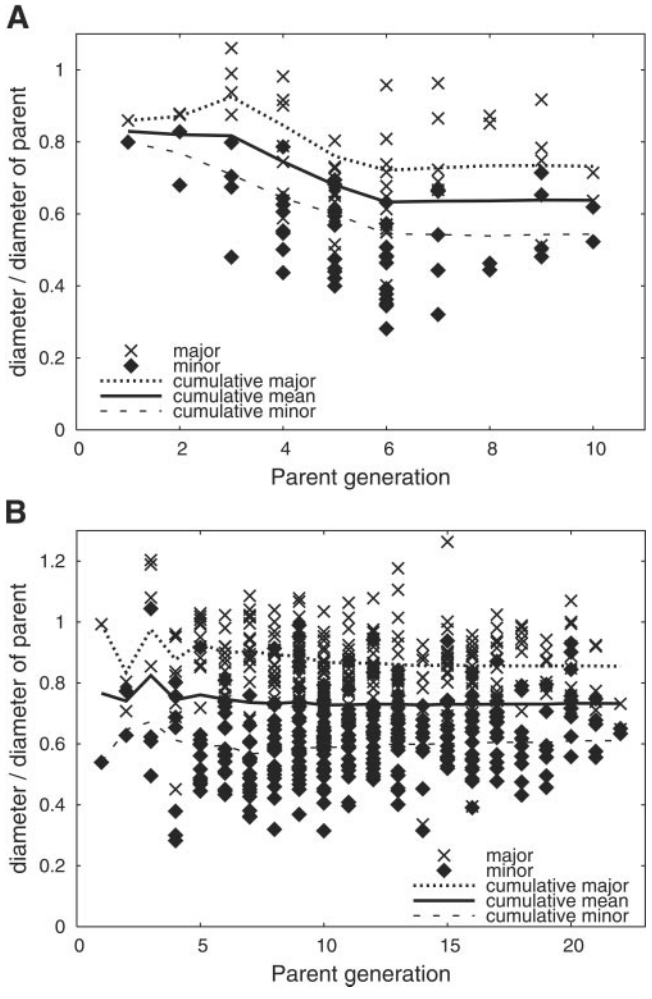

Fig. 2. Ratio of child to parent diameter for minor and major branches at each branch division plotted against parent generation for human (*A*) and ovine (*B*) airways from MDCT. Individual branch values are plotted for major branches (x) and for minor branches (◆). Three lines on each graph plot the cumulative mean values (mean for all branches up to and including the current generation) for the major child ratio, minor child ratio, and total mean.

Minor and major branch classification is determined by branch diameter; therefore the mean ratios of minor to major diameter (D_{minor}/D_{major}) must be ≤ 1. D_{minor}/D_{major} for the sheep airway tree (0.72 ± 0.18) is smaller than for the human (0.85 ± 0.14). The human value is within the range measured in previous studies (25, 31, 43), and the sheep value is slightly less than the smallest value in the range (31). Phalen et al. (25) measured generally smaller ratios in dog, rabbit, and rat airways.

The mean ratio of length to diameter (L/D) for the human MDCT airways is 3.04 ± 2.20, which sits in the middle of the range of published values (31, 43). L/D for minor branches is larger than for major branches. This is consistent with the finding of Phillips and Kaye (27); however, the difference between major and minor ratios is larger in the current study. L/D calculated for the sheep MDCT airways is much smaller than for the human (2.69 ± 1.76), but it is larger than the range of minor branch L/D ratios calculated by Phillips and Kaye (27) for the dog, rat, and hamster airways using data from Raabe et al. (29).

The ratio of branch length to parent branch length (L/L_{parent},) is >1 for the MDCT airways in both species. Krause et al. (17) calculated L/L_{parent} as 1.65 ± 3.25 for the dog lung, with 58.8% of the branches shorter than the parent branch. The MDCT-based human and sheep airways have similar percentages of branches shorter than the parent branch, and both data sets have relatively large standard deviations. This is consistent with previous studies where it has been observed that branch length does not decrease as uniformly as the diameter (27, 43). The mean ratio of child airway lengths (L_1/L_2, where L_1/L_2) is smaller in the human than the sheep. The mean values are very close to measurements by Weibel (43) and Phalen et al. (25).

MDCT Airways: Fitting

The initial linear mesh of the human MDCT airway (Fig. 3*A*) comprised 122 nodes and 121 elements that were fitted to 1,871 centerline data points. The root mean square (RMS) error between the centerline data and the initial mesh was 2.215 mm, and the RMS error of the fitted mesh (Fig. 3*B*) was 0.402 mm after five fitting iterations. Nine hundred thirty-nine nodes and 933 elements were fit to 7,784 centerline data points for the sheep MDCT airway mesh. The RMS error for the initial mesh (Fig. 4*A*) was 1.806 mm, which reduced to 0.340 mm for the fitted mesh (Fig. 4*B*) after nine iterations.

The RMS errors for the initial diameters (equal to mean airway diameter) were 1.107 mm (human) and 0.339 mm (sheep); the fitted diameter meshes (Figs. 3*C* and 4*C*) had RMS errors of 0.158 mm (human) and 0.132 mm (sheep).

Model Airways Generated by Branching Algorithm

The third column in both Tables 1 and 2 lists the geometric properties calculated for the airway models that were generated into the volume meshes of the five human lobes (Table 1) and

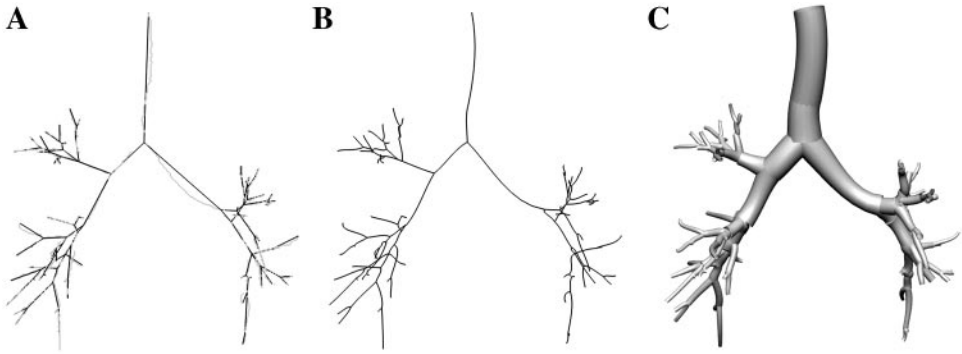

Fig. 3. Steps in the generation of an MDCT-based model of the human bronchial airways. Initial linear centerline mesh (heavy line) that directly joins the bifurcation points, and discrete centerline points (thin line) to which curvature is fit (*A*), fitted high-order centerline mesh that joins the bifurcation points with 1D curvilinear elements (*B*), airway mesh with centerline curvature and fitted circular diameters (*C*).

two sheep lungs (Table 2). The human model (including MDCT-based airways) has 29 generations, 29 Horsfield orders, and 11 Strahler orders, compared with 46 generations, 46 Horsfield orders, and 10 Strahler orders in the MDCT-based + generated sheep airway model.

The mean branching angle (θ) for the generated human tree is larger than published values. Figure 5 shows that this is influenced largely by the peripheral branches. From Strahler order 4 to 9, θ is equal to or less than the theoretical ideal (9). The model θ increases toward the periphery, as described for the upper orders (10), and has large standard deviations.

Log plots of number of branches, length, and diameter used to calculate R_bS, R_lS, and R_dS in the human model are shown in Fig. 6 and values are listed in Table 1. Further values of R_bS are listed in Table 3 for generation of human airway models into two lungs rather than five lobes and for initiating from the two major bronchi rather than from all of the peripheral MDCT model airways. In both cases, R_bS decreases relative to its value for model generation from all MDCT airways into separate lobes. R_bS also decreases for generation from the small initial branch set in the sheep (Table 3).

The human lung lobe volume mesh is shown in Fig. 7*A*, and the full generated human model in Fig. 7*B*. The lobes and lobar airways are differentiated by color: the right upper lobe is green, right middle lobe is red, right lower lobe is blue, left upper lobe is yellow, and left lower lobe is orange. The corresponding models for the sheep lung are shown in Fig. 7, *C-E*, with the lungs and airways colored light brown for the right lung and dark brown for the left lung. Figure 8 shows close up views of each airway model, highlighting the difference in geometry between the two species.

DISCUSSION

Bronchial airway models that are employed for functional simulations have generally been idealizations of real airway geometry based on measurements from a small number of airway casts (10, 43). In contrast, three-dimensional computational fluid dynamics simulations use models with a high level of anatomic detail specific to an individual (22), but because of the fine resolution of the three-dimensional mesh these types of models are usually limited to a relatively small number of airways. A recent study by Schmidt et al. (33) derived a digital reference model of the human bronchial tree over 17 Horsfield orders, using CT scanning of an airway cast. Although this study has provided further insight into airway branching geometry, it is not a method that can be used to generate geometric models for the entire in vivo conducting airway tree. In the current study a method has been applied to generate airway centerline models that are specific to an individual.

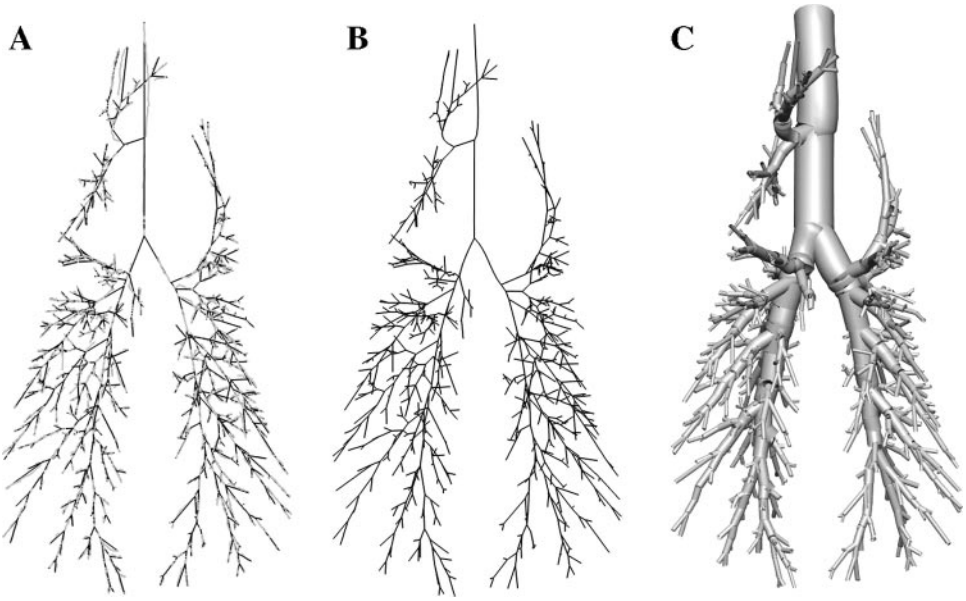

Fig. 4. Steps in the generation of an MDCT-based model of the ovine bronchial airways. Initial linear centerline mesh that directly joins the bifurcation points (*A*), fitted high-order centerline mesh that joins the bifurcation points with 1D curvilinear elements (*B*), airway mesh with centerline curvature and fitted circular diameters (*C*).

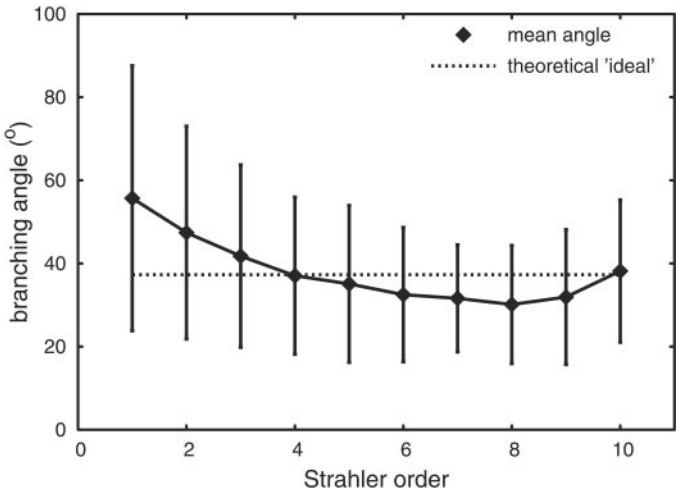

Fig. 5. Mean branching angle and SD plotted against Strahler order for the full human model airway tree (MDCT-based airways and airways generated using a volume-filling algorithm). Theoretical "ideal" angle proposed by Horsfield and Cumming (9) is plotted as a dashed line.

Centerline models that incorporate the airway diameters by integration of governing equations over the cross-sectional area are tractable for functional predictions in the entire conducting airway system (38, 39). The application of this type of one-dimensional model is therefore wide and varied: from predictions of airway mechanics (40) to the dynamics of gas mixing (38), or for tracing airway paths for virtual bronchoscopy (15). In the current study, models of the bronchial airway system have been developed from MDCT data segmented from human and sheep scans. The MDCT-based measures of the geometry of the human and sheep airway were first analyzed to verify that the segmentation methods produce airway structures that are consistent with previous morphometric studies. The MDCT airway analysis has provided new data on the geometry of the sheep bronchial tree. Airway models have been developed directly from the MDCT data by *1*) fitting the model mesh centerlines and diameters to data extracted from an XML description of the airway geometry and *2*) using a mathematical algorithm to generate bifurcating trees within MDCT-based volume meshes. The geometries of the full conducting airway systems are generally consistent with available anatomic measures.

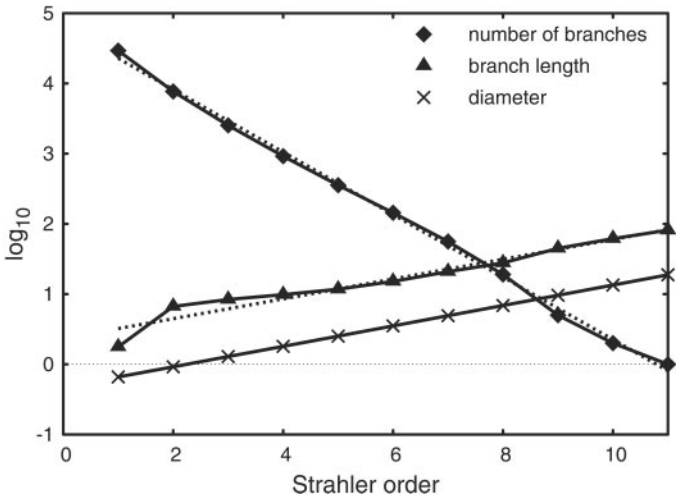

Fig. 6. Log plots for calculation of Strahler-based ratios (R_bS, R_lS, and R_dS) for the full human model airway tree (MDCT-based airways + airways generated using a volume-filling algorithm). Regression lines for each plot are drawn as dashed lines. The trachea is at order 11.

Table 3. *R_bS for different generation scenarios*

	Human	Sheep
Lobes, all MDCT airways	2.80	
Lungs, all MDCT airways	2.59	3.19
Lungs, from main bronchi	2.44	3.09
Length limit = 3 mm		3.61

Airways are generated: into separate lobes (human) or lungs (human and sheep) starting from all peripheral MDCT-based airways; into separate lungs starting from the left and right main bronchus (human) or from the left and right main bronchus and the right apical lobe bronchus (sheep); and using a length limit of 3 mm in the sheep lung.

CT-Based Measurements of Airway Geometry

Significantly more branches (by generation count) were segmented from the sheep MDCT scans than from the human scans. Classification of the branches by generation shows that airways up to *generations 10* and *23* were segmented from the human and sheep, respectively. Monopodial branching in the sheep gives rise to a large number of relatively short segments that are classified as an individual branch by the generation or Horsfield ordering schemes but that may not constitute a separate branch in the Strahler ordering scheme. The number of Strahler classified branches (567) is therefore significantly less than the number of branches classified by generation (933) in the MDCT sheep airways.

The end of a parent branch and start of the child branches in the MDCT airway trees was defined to be at the common bifurcation point. Estimates of branch lengths are therefore the distances between the bifurcation points, which is consistent with the approach used in previous studies. This definition may not be appropriate for some monopodial branching divisions in the sheep bronchial tree. When the minor branch has a large branching angle and much smaller diameter than the parent branch, then the minor child branch originates from the wall of the parent branch and not from the bifurcation point that lies on the centerline of the parent. The consequence of measuring from the common bifurcation point is that the branch lengths may be overestimated (and therefore L/D overestimated), particularly for the minor branches. In future descriptions of the monopodial airway tree, or for its implementation in simulation studies, it may be more appropriate to use different locations for the end of a parent branch and the start of a child branch, or in a Strahler-ordered tree to have a child branch arising directly from the wall at some location along the length of the parent.

The mean branching plane rotation angle for the human (ϕ in Table 1) is close to the mean value of 79° measured by Sauret et al. (31), whereas the sheep ϕ (Table 2) is very close to the 90° rotation that has been observed in human studies of airway casts (13). The number of bifurcations for which the branching angle could be calculated in the sheep was far greater than for the human airway tree. Segmentation of lower order branches in the human tree may show that the smaller ϕ

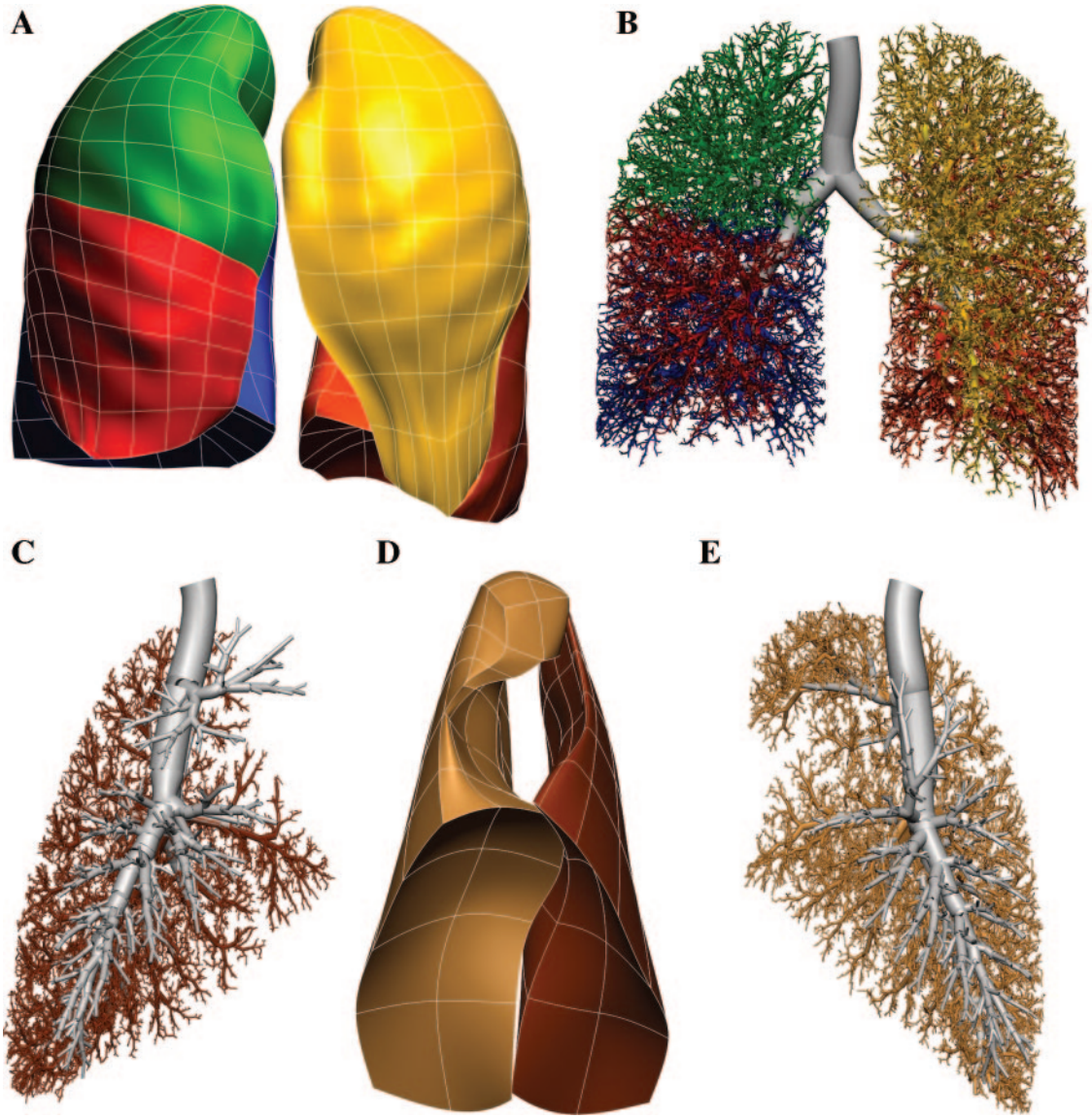

Fig. 7. Finite element volume meshes and volume-filling airway models. Volume meshes of the human right upper (green), right middle (red), right lower (blue), left upper (yellow), and left lower (orange) lobes (*A*), generated human airway model with lobar airways colored as in *A* and MDCT-based airways in gray (*B*), MDCT-based ovine airways in gray and left lung generated airways in dark brown (*C*), viewed from the right volume mesh for the right (light brown) and left (dark brown) ovine lungs (*D*), generated airways for the right lung shown in light brown, viewed from the left (*E*).

is valid for the largest airways, but that it is closer to 90° for the smaller airways.

Model Fitting to MDCT Data

Translation of the XML tree file into an initial mesh, centerline data points, and diameter data has been developed as an automated process that requires minimal user involvement. This means that the derivation of bronchial tree models from scan data can be accomplished quickly for a large number of data sets. The translation of the XML airway tree description into an initial linear mesh for centerline fitting produces an initial geometry that is well constructed for quick convergence of the fitting solution. The centerline fits for both models result in small RMS errors and each requires a maximum of nine solution iterations to reach convergence. By employing high-order elements for the MDCT airway model description, only a single element is required for each airway and the airway curvature is represented efficiently. The curvilinear centerline model differs from previous comparable one-dimensional models that have used straight cylindrical elements. The advantage of including curvature is that a better spatial description of the airway is achieved such that relating the current one-dimensional models to three-dimensional models developed from the same data set is straightforward. This becomes important when coupling different functional models: for example, compression of the airways in the one-dimensional airway tree coupled to soft tissue deformation of the three-dimensional lung.

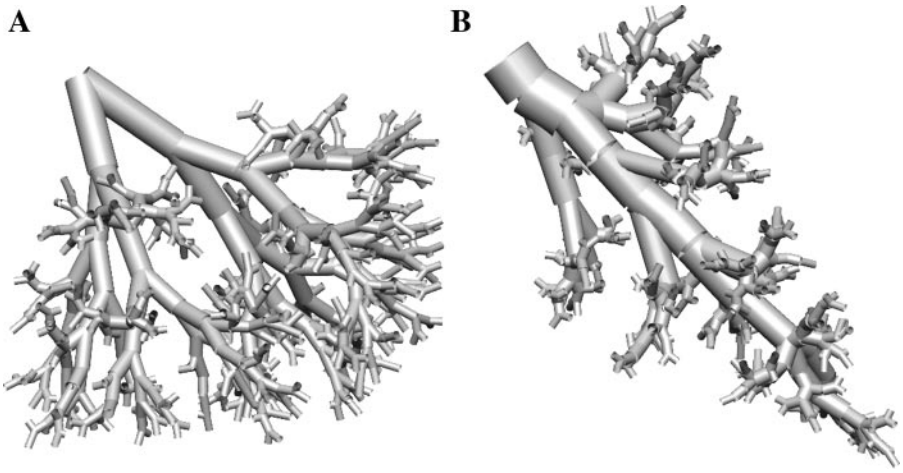

Fig. 8. Close view of generated airways in human (*A*) and ovine (*B*) airway models. Each image displays airways that have been generated into the respective species host lung; in each case a portion of the airway model has been isolated that is peripheral to the MDCT-defined airways.

Model Generation by Branching Algorithm

Tawhai et al. (37) conducted a sensitivity analysis of the airway branching algorithm and a comparison of geometry against previous airway models. The current study does not seek to reproduce this analysis. The branching algorithm used for model generation in the current study differs from the original algorithm in the spacing and density of seed points and in grouping seed points with the closest peripheral branches throughout the generation process.

Tawhai et al. (37) used a very dense set of randomly distributed seed points. In the current study, the number of seed points is equal to the estimated number of transitional bronchioles. A criteria used in the original algorithm was termination of a branching path when the number of points in a set was less than a minimum value that represented the mean acinus volume. This is equivalent to the condition used in the current study that a path terminates if only a single point remains in a point set. That is, the larger number of points in the original algorithm and the single point in the current study both represent a single pulmonary acinus. The advantage of using only a single seed point per transitional bronchiole/acinus is that generation of the tree is far quicker, with no negative impact on the generated model geometry. Spacing the seed points in a uniform grid rather than randomly distributing significantly reduces the model computation time, also with no negative impact on the generated model.

The major difference from the original algorithm is that throughout the generation process the seed points are regrouped with the closest peripheral branch. This grouping allows the algorithm to be initiated from any number of predefined airway locations. In the original algorithm the seed points in a single lobe were all allocated to the corresponding lobar bronchus. The points were divided and redivided for branching, as described in METHODS, but in contrast to the current study, seed points could only be associated with branches that were peripheral to a higher order branch to which the seed points had previously been grouped. By reallocating the seed points after generation of a new set of branches this constraint is relaxed. The major effect of this change appears to be on θ. In the models generated by Tawhai et al. (37), θ did not increase toward the periphery, whereas in the current study, θ does increase with decreasing order (Fig. 5). As the number of bifurcations increases, more of the airway paths terminate by length limitation, and their seed points are reassigned. The reassigned points cause a larger dispersal of the centers of mass, and hence the tree "spreads" out. Mean θ for the entire human tree is therefore larger than published values, but this is influenced largely by the branching angles in the peripheral branches (Fig. 5). Branching plane rotation angles (ϕ) for both the human and sheep model were very close to 90°, although the algorithm places no constraint on the plane of branching: the branch orientation is defined entirely by the spatial distribution of the seed points toward which it branches.

Diameters were assigned in the models assuming that $R_dS = R_bS^{1/3}$. Diameters could have been assigned using mean values per generation or order; however, diameter variation within a generation is large (43), and mean values per order are not available for the sheep airways. Diameters could also have been estimated by assuming a fixed value for L/D; however, for branches with a shorter parent branch length (22% of the human airways and 23% of the sheep airways) the diameter would be larger than that of its parent, and for very short branches the diameter would be correspondingly small. A limitation of using the simple power law to assign diameters is that all diameters in a given Strahler order are identical. A more sophisticated method could be employed, for example adapting the diameters to ensure that they match measured values for parent to child or sibling ratios. The diameters were not manipulated in this way in the models presented here so that the comparison of diameter-based ratios from the models with those from anatomic studies would be clear. Ratios that were calculated for the generated model airways using only diameter values (D_{minor}/D_{parent}, D_{major}/D_{parent}, D/D_{parent}) are close to published values for the human lung (17, 27, 31, 43) and MDCT-based measures in the current study for the sheep. The average effect of the simple diameter rule is therefore adequate for diameter-based ratios.

Mean L/D for the human and sheep models are consistent with corresponding values for the MDCT airways. L/D_{minor} and L/D_{major} for the sheep follow the trend of the MDCT airways ($L/D_{minor} > L/D > L/D_{major}$), but they do not vary as much from the total mean L/D. The situation for the human model airways is reversed: $L/D_{minor} < L/D < L/D_{major}$. This highlights a limitation of the simplistic diameter rule for the

human airway. For simulation studies, the detail of the human airway tree may therefore be better represented using R_dH to assign the diameters than R_dS or may require introduction of additional constraints on the relationship between the diameter of a branch and that of its parent or sibling.

Branching, length, and diameter ratios were calculated using both Horsfield and Strahler ordering for the human model and using only Strahler ordering for the sheep model. Figure 6 illustrates the log plot used to calculate the Strahler ratios. Ratios calculated using Strahler orders are more accurate than those calculated from Horsfield ordering because the Strahler log plots are more linear (13). This is especially true for the length ratio, for which the R^2 value for R_bS is much closer to 1 than for R_bH. All of the Strahler-based ratios are within the published range (12) for the human airway models, but the sheep model has smaller values of R_bS and R_dS than published (12). That is, the asymmetry of the human airway model is appropriate but the sheep airway model branching pattern is not quite as asymmetric as published studies propose.

A number of different hypotheses were tested to determine their influence on branching asymmetry, in particular to probe whether the higher asymmetry in the generated sheep model results from the geometry of the sheep lung or from the far more extensive initial description of the MDCT airways than for the human and whether increasing the length limit affects the R_bS. Table 3 lists the results of these various tests. Removing the separation of the lungs into lobes caused the human R_bS to decrease from 2.80 to 2.59. Therefore, the constraint imposed by the definition of the lobar surface contributed to the asymmetry of the airway tree. The sheep lung was not segmented into separate lobes: only the volume of the two lungs was defined. Definition of the lobes may therefore increase the sheep model R_bS. Generation of the model from a minimum number of initial branches decreased R_bS for the human and sheep models to a similar extent but not as much as the reduction from removing the lobes. Accurate definition of the initial airways therefore contributed to the model asymmetry, but the contribution was relatively small. The much larger R_bS for the sheep lung therefore cannot be attributed to the more extensive initial airway definition: in each case R_bS for the sheep was considerably larger than R_bS for the human. The shape of the sheep lung therefore appears to be the major contributing factor to the higher branching asymmetry of the generated sheep model relative to the model of the human lung.

Lipsett (18) proposed a much longer terminal bronchiole length in the sheep lung (6.8 mm) than has been measured for humans. Increasing the length limit to 3 mm increased R_bS to 3.61, but this was at the expense of increasing the number of generations to close to 60. Without physiological evidence to support this large number of generations, it would appear that the 2-mm length limit used in the current study, on the basis of human anatomy, is more suitable.

The sheep model used a seed point density that was more than twice the density used for the human lung. If each seed point represents a single acinus, then the result is that the number of acini in the sheep model is approximately the same as the number in the human lung but each with half the volume. On the basis of comparative sizes of acini in other mammalian species (30), the sheep acinus would be expected to be smaller than the human acinus. For $R_bS = 3.55$, with nine Strahler orders the number of terminal bronchioles would be 25,000, which is close to the number used in the current study.

The work described here demonstrated the consistency of the human MDCT-segmented airway structure with published anatomic measurements for the majority of experimental values and hence shows that MDCT airway imaging can generate reasonable statistics on airway geometry. Very few published values were available for comparison with the sheep MDCT tree, therefore the sheep measurements provide a new set of anatomic data. The human and sheep spatially distributed models are generally consistent with previously published values and with the measurements presented here from MDCT. A further test of the ability of the airway generation algorithm would be to generate models into other nonhuman species, such as dog, rabbit, or rat, for which there are more extensive anatomic data. However, as demonstrated here, the definition of the individual lobes is important for the airway tree geometry, but the imaging segmentation algorithms necessary to separate these structures is not currently available for all species.

GRANTS

This work was supported by The Royal Society of New Zealand Marsden Grant 01-U0A-070 MIS, the Maurice Paykel Postdoctoral Fellowship, and National Institutes of Health Bioengineering Research Partnership Grant R01-HL-064368.

REFERENCES

1. **Albert MS, Cates GD, Driehuys B, Happer W, Saam B, Springer CS Jr, and Wishnia A.** Biological magnetic resonance imaging using laser-polarized 129Xe. *Nature* 370: 199–201, 1994.
2. **Chulho W, Chon D, Tajik J, Tran BQ, Robinswood GB, Beck KC, and Hoffman EA.** CT-based assessment of regional pulmonary microvascular blood flow parameters. *J Appl Physiol* 94: 2483–2493, 2003.
3. **Clough AV, Haworth ST, Roerig DL, Hoffman EA, and Dawson CA.** Influence of gravity on radiographic contrast material-based measurements of regional blood flow distribution. *Acad Radiol* 10: 128–138, 2003.
4. **Fernandez JW, Mithraratne P, Tawhai MH, and Hunter PJ.** Geometric fitting and customization of anatomically based cubic Hermite finite element volume meshes. *Biomech Model Mechanobiol* 2: 139–155, 2004.
5. **Haefeli-Bleuer B and Weibel ER.** Morphometry of the human pulmonary acinus. *Anat Rec* 220: 401–414, 1988.
6. **Herman GT and Carvalho BM.** Multiseeded segmentation using fuzzy connectedness. *IEEE Trans Pattern Anal Machine Intelligence* 23: 460–474, 2001.
7. **Hoffman EA and McLennan G.** Assessment of the pulmonary structure-function relationship and clinical outcomes measures: quantitative volumetric CT of the lung. *Acad Radiol* 4: 758–776, 1997.
8. **Hoffman EA, Reinhardt JM, Sonka M, Simon BA, Guo J, Saba O, Chon D, Samrah S, Shikata H, Tschirren J, Palagyi K, Beck KC, and McLennan G.** Characterization of the interstitial lung diseases via density-based and texture-based analysis of computed tomography images of lung structure and function. *Acad Radiol* 10: 1104–1118, 2003.
9. **Horsfield K and Cumming G.** Angles of branching and diameters of branches in the human bronchial tree. *Bull Math Biophys* 29: 245–259, 1967.
10. **Horsfield K, Dart G, Olson DE, Filley GF, and Cumming G.** Models of the human bronchial tree. *J Appl Physiol* 31: 207–217, 1971.
11. **Horsfield K, Relea FG, and Cumming G.** Diameters, lengths, and branching ratios in the bronchial tree. *Respir Physiol* 26: 351–356, 1976.
12. **Horsfield K and Thurlbeck A.** Volume of the conducting airways calculated from morphometric parameters. *Bull Math Biol* 43: 101–109, 1981.
13. **Horsfield K.** Anatomical factors influencing gas mixing and distribution. In: *Gas Mixing and Distribution in the Lung*, edited by Engel LA and Paiva M. NY: Dekker, 1985.
14. **Hu S, Hoffman EA, and Reinhardt JM.** Automatic lung segmentation for accurate quantitation of volumetric X-ray CT images. *IEEE Trans Med Imaging* 20: 490–498, 2001.

15. **Kiraly AP, Higgins WE, McLennan G, Hoffman EA, and Reinhardt JM.** Three-dimensional human airway segmentation methods for clinical virtual bronchoscopy. *Acad Radiol* 9: 1153–1168, 2002.
16. **Kitaoka H, Takaki R, and Suki B.** A three-dimensional model of the human airway tree. *J Appl Physiol* 87: 2207–2217, 1999.
17. **Krause E, Bandt C, Schulz A, and Schulz H.** Fractal exponents for the upper airways of mammalian lungs. *Computat Stat Data Analysis* 20: 583–590, 1995.
18. **Lipsett J.** Analysis of the conducting airway system in the lung: a new method combining morphometry with mathematical modeling for airway classification. *Anat Rec* 266: 51–57, 2002.
19. **Lipson DA, Roberts DA, Hansen-Flaschen J, Gentile TR, Jones G, Thompson A, Dimitrov IE, Palevsky HI, Leigh JS, Schnall M, and Rizi RR.** Pulmonary ventilation and perfusion scanning using hyperpolarized helium-3 MRI and arterial spin tagging in healthy normal subjects and in pulmonary embolism and orthotopic lung transplant patients. *Magn Reson Med* 47: 1073–1076, 2002.
20. **Marcucci C, Nyhan D, and Simon BA.** Distribution of pulmonary ventilation using Xe-enhanced computed tomography in prone and supine dogs. *J Appl Physiol* 90: 421–430, 2001.
21. **Miller GW, Altes TA, Brookeman JR, De Lange EE, and Mugler JP 3rd.** Hyperpolarized (3)He lung ventilation imaging with B(1)-inhomogeneity correction in a single breath-hold scan. *MAGMA* 16: 218–226, 2004.
22. **Nowak N, Kakade PP, and Annapragada AV.** Computational fluid dynamics simulation of airflow and aerosol deposition in human lungs. *Ann Biomed Eng* 31: 374–390, 2003.
23. **Palágyi K, Sorantin E, Balogh E, Kuba A, Halmai C, Erdohelyi B, and Hausegger K.** A sequential 3D thinning algorithm and its medical applications. In: *17th Int Conf Information Processing in Medical Imaging, IPMI 2001, Davis, CA, USA. Lecture Notes in Computer Science 2082*, 2001, p. 409–415.
24. **Palágyi K, Tschirren J, and Sonka M.** Quantitative analysis of intrathoracic airway trees: methods and validation. In: *18th Int Conf Information Processing in Medical Imaging, IPMI 2003, Ambleside, UK, Lecture Notes in Computer Science 2732.* Springer, 2003, p. 222–233.
25. **Phalen RF, Yeh HC, Schum GM, and Raabe OG.** Application of an idealized model to morphometry of the mammalian tracheobronchial tree. *Anat Rec* 190: 167–176, 1978.
26. **Phillips CG, Kaye SR, and Schroter RC.** A diameter-based reconstruction of the branching pattern of the human bronchial tree. Part I. Description and application. *Respir Physiol* 98: 193–217, 1994.
27. **Phillips CG and Kaye SR.** Diameter-based analysis of the branching geometry of four mammalian bronchial trees. *Respir Physiol* 102: 303–316, 1995.
28. **Polak AG and Lutchen KR.** Computational model for forced expiration from asymmetric normal lungs. *Ann Biomed Eng* 31: 891–907, 2003.
29. **Raabe OG, Yeh HC, Schum GM, and Phalen RF.** *Tracheobronchial Geometry: Human, Dog, Rat, Hamster*. Albuquerque, NM: Lovelace Foundation for Medical Education and Research, 1976.
30. **Sapoval B, Filoche M, and Weibel ER.** Smaller is better—but not too small: a physical scale for the design of the mammalian pulmonary acinus. *Proc Natl Acad Sci USA* 99: 10411–10416, 2002.
31. **Sauret V, Halson PM, Brown IW, Fleming JS, and Bailey AG.** Study of the three-dimensional geometry of the central conducting airways in man using computed tomographic (CT) images. *J Anat* 200: 123–134, 2000.
32. **Schlesinger RB and McFadden LA.** Comparative morphometry of the upper bronchial tree in six mammalian species. *Anat Rec* 199: 99–108, 1981.
33. **Schmidt A, Zidowitz S, Kriete A, Denhard T, Krass S, and Peitgen H.** A digital reference model of the human bronchial tree. *Comput Med Imaging Graph* 28: 203–211, 2004.
34. **Shi L, Hoffman EA, and Reinhardt JM.** Segmentation of the ovine lung in 3D CT images. In: *SPIE Medical Imaging Proc of SPIE* 5369: 2004.
35. **Simon BA, Marcucci C, Fung M, and Lele SR.** Parameter estimation and confidence intervals for Xe-CT ventilation studies: a Monte Carlo approach. *J Appl Physiol* 84: 709–716, 1998.
36. **Tajik K, Chon D, Won C, Tran BQ, and Hoffman EA.** Subsecond multisection CT of regional pulmonary ventilation. *Acad Radiol* 9: 130–146, 2002.
37. **Tawhai MH, Pullan AJ, and Hunter PJ.** Generation of an anatomically based three-dimensional model of the conducting airways. *Ann Biomed Eng* 28: 793–802, 2000.
38. **Tawhai MH and Hunter PJ.** Multibreath washout analysis: modelling the influence of conducting airway asymmetry. *Respir Physiol* 127: 249–258, 2001.
39. **Tawhai MH and Hunter PJ.** Modeling water vapor and heat transfer in the normal and the intubated airway. *Ann Biomed Eng* 34: 609–622, 2004.
40. **Tgavalekos NT, Venegas JG, Suki B, and Lutchen KR.** Relation between structure, function, and imaging in a three-dimensional model of the human lung. *Ann Biomed Eng* 31: 363–373, 2003.
41. **Tschirren J.** *Segmentation, Anatomical Labeling, Branchpoint Matching, And Quantitative Analysis of Human Airway Trees in Volumetric CT Images* (PhD thesis). Iowa City, IA: University of Iowa, 2003.
42. **Tschirren J, Hoffman EA, McLennan G, and Sonka M.** Airway tree segmentation using adaptive regions of interest. In: *SPIE Medical Imaging, San Diego, CA, USA February 14–19 Proceedings of SPIE* 5369: 2, 2004.
43. **Weibel ER.** *Morphometry of the Human Lung*. Berlin: Springer-Verlag, 1963.
44. **Zhang L, Hoffman EA, and Reinhardt JM.** Atlas-driven lung lobe segmentation in volumetric X-ray CT images. In: *SPIE Medical Imaging, San Diego, CA, USA Proceedings of SPIE* 5032: 309–319, 2003.
45. **Zheng J, Leawoods JC, Nolte M, Yablonskiy DA, Woodard PK, Laub G, Gropler RJ, and Conradi MS.** Combined MR proton lung perfusion/angiography and helium ventilation: potential for detecting pulmonary emboli and ventilation defects. *Magn Reson Med* 47: 433–438, 2002.